FERMILAB-PUB-20-666-ND

arXiv:2012.07928v2 [hep-ex] 27 Mar 2021

High-performance Generic Neutrino Detection in a LArTPC near the Earth's Surface with the MicroBooNE Detector

P. Abratenko,[36] M. Alrashed,[15] R. An,[14] J. Anthony,[4] J. Asaadi,[35] A. Ashkenazi,[19] S. Balasubramanian,[39] B. Baller,[11] C. Barnes,[20] G. Barr,[24] V. Basque,[18] L. Bathe-Peters,[13] O. Benevides Rodrigues,[32] S. Berkman,[11] A. Bhanderi,[18] A. Bhat,[32] M. Bishai,[2] A. Blake,[16] T. Bolton,[15] L. Camilleri,[10] D. Caratelli,[11] I. Caro Terrazas,[9] R. Castillo Fernandez,[11] F. Cavanna,[11] G. Cerati,[11] Y. Chen,[1] E. Church,[25] D. Cianci,[10] J. M. Conrad,[19] M. Convery,[29] L. Cooper-Troendle,[39] J. I. Crespo-Anadón,[10,6] M. Del Tutto,[11] D. Devitt,[16] R. Diurba,[21] L. Domine,[29] R. Dorrill,[14] K. Duffy,[11] S. Dytman,[26] B. Eberly,[31] A. Ereditato,[1] L. Escudero Sanchez,[4] J. J. Evans,[18] G. A. Fiorentini Aguirre,[30] R. S. Fitzpatrick,[20] B. T. Fleming,[39] N. Foppiani,[13] D. Franco,[39] A. P. Furmanski,[21] D. Garcia-Gamez,[12] S. Gardiner,[11] G. Ge,[10] S. Gollapinni,[34,17] O. Goodwin,[18] E. Gramellini,[11] P. Green,[18] H. Greenlee,[11] W. Gu,[2] R. Guenette,[13] P. Guzowski,[18] L. Hagaman,[39] E. Hall,[19] P. Hamilton,[32] O. Hen,[19] G. A. Horton-Smith,[15] A. Hourlier,[19] E.-C. Huang,[17] R. Itay,[29] C. James,[11] J. Jan de Vries,[4] X. Ji,[2] L. Jiang,[37] J. H. Jo,[39] R. A. Johnson,[8] Y.-J. Jwa,[10] N. Kamp,[19] N. Kaneshige,[3] G. Karagiorgi,[10] W. Ketchum,[11] B. Kirby,[2] M. Kirby,[11] T. Kobilarcik,[11] I. Kreslo,[1] R. LaZur,[9] I. Lepetic,[27] K. Li,[39] Y. Li,[2] B. R. Littlejohn,[14] D. Lorca,[1] W. C. Louis,[17] X. Luo,[3] A. Marchionni,[11] C. Mariani,[37] D. Marsden,[18] J. Marshall,[38] J. Martin-Albo,[13] D. A. Martinez Caicedo,[30] K. Mason,[36] A. Mastbaum,[27] N. McConkey,[18] V. Meddage,[15] T. Mettler,[1] K. Miller,[7] J. Mills,[36] K. Mistry,[18] A. Mogan,[34] T. Mohayai,[11] J. Moon,[19] M. Mooney,[9] A. F. Moor,[4] C. D. Moore,[11] L. Mora Lepin,[18] J. Mousseau,[20] M. Murphy,[37] D. Naples,[26] A. Navrer-Agasson,[18] R. K. Neely,[15] P. Nienaber,[28] J. Nowak,[16] O. Palamara,[11] V. Paolone,[26] A. Papadopoulou,[19] V. Papavassiliou,[22] S. F. Pate,[22] A. Paudel,[15] Z. Pavlovic,[11] E. Piasetzky,[33] I. D. Ponce-Pinto,[10] D. Porzio,[18] S. Prince,[13] X. Qian,[2] J. L. Raaf,[11] V. Radeka,[2] A. Rafique,[15] M. Reggiani-Guzzo,[18] L. Ren,[22] L. Rochester,[29] J. Rodriguez Rondon,[30] H. E. Rogers,[5] M. Rosenberg,[26] M. Ross-Lonergan,[10] B. Russell,[39] G. Scanavini,[39] D. W. Schmitz,[7] A. Schukraft,[11] W. Seligman,[10] M. H. Shaevitz,[10] R. Sharankova,[36] J. Sinclair,[1] A. Smith,[4] E. L. Snider,[11] M. Soderberg,[32] S. Söldner-Rembold,[18] S. R. Soleti,[24,13] P. Spentzouris,[11] J. Spitz,[20] M. Stancari,[11] J. St. John,[11] T. Strauss,[11] K. Sutton,[10] S. Sword-Fehlberg,[22] A. M. Szelc,[18] N. Tagg,[23] W. Tang,[34] K. Terao,[29] C. Thorpe,[16] M. Toups,[11] Y.-T. Tsai,[29] S. Tufanli,[39] M. A. Uchida,[4] T. Usher,[29] W. Van De Pontseele,[24,13] B. Viren,[2] M. Weber,[1] H. Wei,[2] Z. Williams,[35] S. Wolbers,[11] T. Wongjirad,[36] M. Wospakrik,[11] W. Wu,[11] E. Yandel,[3] T. Yang,[11] G. Yarbrough,[34] L. E. Yates,[19] H. W. Yu,[2] G. P. Zeller,[11] J. Zennamo,[11] and C. Zhang[2]

(The MicroBooNE Collaboration)*

[1] *Universität Bern, Bern CH-3012, Switzerland*
[2] *Brookhaven National Laboratory (BNL), Upton, NY, 11973, USA*
[3] *University of California, Santa Barbara, CA, 93106, USA*
[4] *University of Cambridge, Cambridge CB3 0HE, United Kingdom*
[5] *St. Catherine University, Saint Paul, MN 55105, USA*
[6] *Centro de Investigaciones Energéticas, Medioambientales y Tecnológicas (CIEMAT), Madrid E-28040, Spain*
[7] *University of Chicago, Chicago, IL, 60637, USA*
[8] *University of Cincinnati, Cincinnati, OH, 45221, USA*
[9] *Colorado State University, Fort Collins, CO, 80523, USA*
[10] *Columbia University, New York, NY, 10027, USA*
[11] *Fermi National Accelerator Laboratory (FNAL), Batavia, IL 60510, USA*
[12] *Universidad de Granada, Granada E-18071, Spain*
[13] *Harvard University, Cambridge, MA 02138, USA*
[14] *Illinois Institute of Technology (IIT), Chicago, IL 60616, USA*
[15] *Kansas State University (KSU), Manhattan, KS, 66506, USA*
[16] *Lancaster University, Lancaster LA1 4YW, United Kingdom*
[17] *Los Alamos National Laboratory (LANL), Los Alamos, NM, 87545, USA*
[18] *The University of Manchester, Manchester M13 9PL, United Kingdom*
[19] *Massachusetts Institute of Technology (MIT), Cambridge, MA, 02139, USA*
[20] *University of Michigan, Ann Arbor, MI, 48109, USA*
[21] *University of Minnesota, Minneapolis, MN, 55455, USA*
[22] *New Mexico State University (NMSU), Las Cruces, NM, 88003, USA*
[23] *Otterbein University, Westerville, OH, 43081, USA*
[24] *University of Oxford, Oxford OX1 3RH, United Kingdom*
[25] *Pacific Northwest National Laboratory (PNNL), Richland, WA, 99352, USA*
[26] *University of Pittsburgh, Pittsburgh, PA, 15260, USA*

This document was prepared by MicroBooNE Collaboration using the resources of the Fermi National Accelerator Laboratory (Fermilab), a U.S. Department of Energy, Office of Science, HEP User Facility. Fermilab is managed by Fermi Research Alliance, LLC (FRA), acting under Contract No. DE-AC02-07CH11359.

[27] Rutgers University, Piscataway, NJ, 08854, USA
[28] Saint Mary's University of Minnesota, Winona, MN, 55987, USA
[29] SLAC National Accelerator Laboratory, Menlo Park, CA, 94025, USA
[30] South Dakota School of Mines and Technology (SDSMT), Rapid City, SD, 57701, USA
[31] University of Southern Maine, Portland, ME, 04104, USA
[32] Syracuse University, Syracuse, NY, 13244, USA
[33] Tel Aviv University, Tel Aviv, Israel, 69978
[34] University of Tennessee, Knoxville, TN, 37996, USA
[35] University of Texas, Arlington, TX, 76019, USA
[36] Tufts University, Medford, MA, 02155, USA
[37] Center for Neutrino Physics, Virginia Tech, Blacksburg, VA, 24061, USA
[38] University of Warwick, Coventry CV4 7AL, United Kingdom
[39] Wright Laboratory, Department of Physics, Yale University, New Haven, CT, 06520, USA
(Dated: March 30, 2021)

Large Liquid Argon Time Projection Chambers (LArTPCs) are being increasingly adopted in neutrino oscillation experiments because of their superb imaging capabilities through the combination of both tracking and calorimetry in a fully active volume. Active LArTPC neutrino detectors at or near the Earth's surface, such as the MicroBooNE experiment, present a unique analysis challenge because of the large flux of cosmic-ray muons and the slow drift of ionization electrons. We present a novel Wire-Cell-based high-performance generic neutrino-detection technique implemented in MicroBooNE. The cosmic-ray background is reduced by a factor of 1.4×10^5 resulting in a 9.7% cosmic contamination in the selected neutrino candidate events, for visible energies greater than 200 MeV, while the neutrino signal efficiency is retained at 88.4% for ν_μ charged-current interactions in the fiducial volume in the same energy region. This significantly improved performance compared to existing reconstruction algorithms, marks a major milestone toward reaching the scientific goals of LArTPC neutrino oscillation experiments operating near the Earth's surface.

The Liquid Argon Time Projection Chamber (LArTPC) [1–4] is an advanced technology to detect neutrinos with its superb imaging capabilities through the combination of both tracking and calorimetry in a fully active volume. Such capabilities make LArTPC detectors attractive to address important unresolved questions in neutrino physics, such as the presence of CP violation in the lepton sector [5, 6], the order of neutrino masses [7], the existence of sterile neutrinos [8] as well as the precise measurements of neutrino-nucleus interactions [9]. In the past two decades, the LArTPC technology has gone through rapid development [10], and detectors with active mass ranging up to 500 tons have been constructed and operated [11–18]. Looking forward, the Short-Baseline Neutrino program (SBN) [19], which consists of three large LArTPCs near the surface, is under construction and partially in operation with the main goal of resolving a class of experimental anomalies in neutrino physics to which the existence of light sterile neutrinos is a possible explanation. Going further, the Deep Underground Neutrino Experiment (DUNE), with multiple 10 kton active mass LArTPC modules as the far detector, is a next generation long-baseline neutrino oscillation experiment aiming to reveal new symmetries of nature [20]. To ensure the success of these future physics programs, the current-generation large LArTPCs, including MicroBooNE [13] and the ProtoDUNEs [18], are critical to develop and demonstrate the full capability of the LArTPC technology.

The SBN program, which the MicroBooNE experiment is part of, utilizes three LArTPCs located along the Booster Neutrino Beam (BNB) [21] at the Fermi National Accelerator Laboratory in Batavia, IL, USA. Inside a single-walled cryostat with a 170 ton capacity, the MicroBooNE detector [13] consists of a 2.56 m (drift direction) × 2.32 m (vertical direction) × 10.36 m (beam direction) active TPC (85 metric tons of liquid argon) for ionization charge detection, and an array of 32 photomultiplier tubes (PMTs) [22] for scintillation light detection. The anode consists of three parallel wire-readout planes, spaced 3 mm apart, with each plane's wires rotated by 60 degrees relative to the other planes and with a 3 mm wire pitch, for a total number of 8256 wires. Ionization electrons from charged particles traveling through the liquid argon drift toward the wire planes at the anode and, near the point where the drift electrons reached the anode, cause detectable currents on a few wires close to the first two "induction" planes and finally on the "collection" plane. The electron drift speed at the operating electric field of 273 V/cm is 1.1 mm/µs, leading to a 2.3 ms drift time for the maximum 2.56 m drift distance. The induced current is amplified and shaped through the custom-designed analog front-end electronics readout [23] operating at 89 K in the liquid argon.

Data recording of candidate neutrino interactions is triggered on a hardware level by each BNB beam spill (within a 1.6 μs time window). Because of the slow drift of ionization electrons which leads to a maximum drift time of 2.3 ms, both TPC and PMT readout windows are extended relative to the beam spill to entirely include both neutrino interactions and spill-in cosmic-ray muon background. For the TPC readout, a digitized waveform

with 9600 samples at a 2 MHz sampling rate, spanning from -1.6 ms to +3.2 ms relative to the trigger, is recorded for each wire. For the PMT readout, a digitized waveform with 1500 samples at a 64 MHz sampling rate covering the beam spill is recorded for each PMT. In addition, self-discriminated PMT readout waveforms, each with 40 samples, are taken during a period of 6.4 ms around the BNB trigger to record cosmic-rays nearby in time. At the nominal BNB intensity of approximately 4×10^{12} protons on target (POT) per spill, MicroBooNE is expected to observe one neutrino interaction inside the TPC active volume per about 600 spills.

The main challenge to detect the BNB neutrinos comes from the large cosmic-ray background because of the near-surface location of the detector. During data acquisition, a software selection is applied that requires those PMT signals in coincidence with a beam spill to exceed a certain threshold, and this reduces the number of recorded events by a factor of 22. Nonetheless, over 95% of the remaining events are still triggered by cosmic rays in coincidence with or arriving just before the beam spill. In addition, at the 5.5 kHz cosmic-ray rate [24], there are on average 26 cosmic-ray muons in the TPC readout window of 4.8 ms for each event. This large cosmic-ray background compromises both the purity and efficiency performance in selecting various neutrino interaction types, as noted in prior work [25–28]. In this letter, we describe a new analysis procedure leading to a significantly improved performance of cosmic-ray background rejection while maintaining a high efficiency in detecting neutrinos. The procedure consists of a series of novel event processing and reconstruction techniques, including (1) offline light reconstruction to reject events triggered by cosmic rays that arrive just before the beam spill, (2) charge-light matching to remove cosmic-rays outside the beam spill, (3) rejection of through-going cosmic-ray muons based on geometry information, (4) rejection of stopped cosmic-ray muons based on calorimetry information, and (5) rejection of events with incorrect charge-light matching. Each technique is delineated as follows.

PMT waveforms are processed offline to reconstruct flashes, representing clusters of PMT signals occurring close in time. For the recorded waveforms triggered by the beam spill, a deconvolution procedure based on the Fast Fourier Transform is performed to remove the PMT readout response. A flash is then formed by requiring that (1) more than two PMTs record activity of greater than 1.5 photoelectrons (PEs), and (2) the total number of PEs recorded by sum of all PMTs is greater than 6 in a 100 ns time bin. Unless another flash is found, the time window for a flash lasts 7.2 μs to include the contribution from the slow component of the scintillation light and to exclude the excess noise (at about 7.3 μs) in the PMT readout system. Similarly, flashes are formed for the self-discriminated waveforms (from a standalone electronics readout) mainly outside the beam spill, where the number of PEs is directly derived from the integral of the waveform after taking into account the single PE response and an extrapolation of the amount of late scintillation light outside the readout window. About 70% of the cosmic rays that pass the software trigger are rejected by requiring at least one reconstructed flash to coincide in time with the beam spill. The rejected events are mainly triggered by the late scintillation light from cosmic-ray muons arriving just before the beam spill.

The TPC data processing procedure includes excess noise removal [29] and signal processing [30]. The signal processing procedure adopts a novel 2D deconvolution technique [30] to extract the ionization charge distribution from the digitized TPC waveforms. This two-dimensional (2D) deconvolution technique significantly improves the charge extraction performance for induction wire planes in comparison with a one-dimensional (1D) deconvolution technique [31] used in previous work. Using this approach, a good agreement between the observed [32] and simulated [30] reconstructed charge in all three wire planes has been achieved.

The 2D charge measurements from the three wire planes are fed into an original tomographic three-dimensional (3D) image reconstruction algorithm, Wire-Cell [33], in which a cross-sectional image in each 2 μs drift-time slice is reconstructed. First, overlapping areas of wire activity, blobs, are created using the wire geometry information. Then, spurious blobs are removed by utilizing the charge information. We use the generic constraints in Wire-Cell to reconstruct a 3D event image independent of its topology (e.g. track or electromagnetic shower). In regions of the detector with non-functional wires [29], a special algorithm reconstructs blobs from activity in just two wire planes. This reduces the previously unusable detector volume by a factor of 10 from 30% to 3% [34]. Additional algorithms such as iterative image reconstruction and clustering are implemented to further remove spurious blobs and to improve the quality of the 3D images [34].

Typically, there are thousands of blobs in a reconstructed 3D event image. They are further grouped into clusters that represent individual physical signals from cosmic-ray muons or a neutrino interaction. In a fully active detector such as a LArTPC, charged particle tracks are expected to leave continuous energy depositions. Therefore, the 3D charge cluster from a single physical signal is identified using a set of algorithms based on connectivity and proximity [34]. Special algorithms are implemented to mitigate the gaps in the 3D image caused by the 3% unusable volume, the imperfect coherent noise removal in the excess noise reduction [29], and the inefficiency of signal processing for the prolonged track topology, i.e. tracks parallel to the drift direction [30]. On the other hand, over-clustering may occur when ionization charges produced at different time

and drift distance but at the same projected position on the anode plane arrive at the anode plane at the same time (same TPC readout time), leading to two separated tracks identified as one single cluster. A special algorithm is created to separate tracks in this case. Figure 1a shows an event image after the 3D clustering.

One particular challenge in the event reconstruction for a LArTPC, compared to other types of tracking calorimeters such as those deployed in NOνA [35], MINERνA [36], and MINOS [37], is that the event topology information from ionization charge and the timing information from scintillation light are decoupled due to the slow drift of ionization electrons. In a typical BNB event, the number of TPC clusters in the TPC readout window is 20–30, and the number of PMT flashes is 40–50. The latter is larger because of the contribution from the LAr volume outside the active TPC. Since the scintillation light is detected by PMTs on a much shorter time scale, the PMT flashes can be used to distinguish each individual TPC signal and to provide its electron drift start time. This is especially useful to select in-beam neutrino activity. A novel many-to-many charge-light matching algorithm is used to find the corresponding PMT flash for each TPC charge cluster [34]. All possible pairs of TPC clusters and PMT flashes are constructed after considering the allowed drift time window for each PMT flash. With each hypothetical cluster-flash pair, the observed PMT light pattern can be compared to the predicted pattern, assuming that the produced light is proportional to the reconstructed charge. The prediction of light at each PMT also considers the acceptance and propagation of the light as a function of the 3D position, which is parameterized by a photon library generated by Geant4 [38, 39]. The compressed sensing technique [40] used in the 3D image reconstruction is again implemented here to select the best hypotheses considering that one cluster can match to zero or one flash and one flash can match to zero, one, or multiple clusters. The average accuracy of the charge-light matching is roughly 95%, evaluated by both Monte Carlo (MC) simulation and data, the latter through a hand-scanning study. Figure 1b shows a data example where the single TPC cluster from a beam ν_e CC interaction candidate is cleanly selected after matching with an in-beam PMT flash.

After charge-light matching, the cosmic-ray muon background, which is mostly outside the beam spill window, is significantly reduced by a factor of 30-40. However, the majority of the remaining in-beam candidates still originate from cosmic-ray muons. Various techniques were developed to reject these cosmic backgrounds with limited impact on the efficiency for identifying neutrino interactions [41].

The largest remaining background is through-going muons that coincides in time with the beam spill, and the number of through-going muons is about 5 times larger than that of neutrino interactions in the active volume after charge-light matching. The identification of through-going muons relies on a precise knowledge of the effective boundary of the TPC active volume. Because of the high rate of cosmic-ray muons traversing the detector volume, the accumulation of positively charged argon ions (i.e. space charge) results in a distorted drift electric field, thus modifying the reconstructed position from the original true position of ionization electrons [42, 43]. The effective boundary shown in Fig. 1b is calibrated with start-time-corrected positions of cosmic-ray muon clusters after charge-light matching. The fiducial boundary used to identify through-going muons is defined as 3 cm inside the effective boundary, which leads to a fiducial volume of 94.2% of the active TPC [41].

The second largest background results from stopped muons, which enter the active volume and stop inside. Stopped muons are identified based on their direction, which is determined by identifying an increase of ionization charge per unit length (dQ/dx) near the end of the track (i.e. Bragg peak). Inspired by the projection matching algorithm [44], a new 3D track trajectory and dQ/dx fitting procedure was developed [41]. First, an initial seed of the trajectory for a TPC cluster is obtained by constructing a Steiner-tree graph [45] from the 3D points in the cluster and finding the shortest paths between extreme points. The Steiner-tree ensures that points associated with the largest charges are included in the initial seed. Then, the best-fit 3D trajectory points with about 6 mm spacing are obtained by minimizing a charge-weighted distance. The charge-weighted distance is constructed to compare the 2D measurements in time-versus-wire views from the three wire planes to the predictions given a 3D trajectory. A numerical solver for large linear systems (BiCGSTAB [46]) is utilized to perform a fast and robust minimization. With the trajectory determined, the dQ/dx associated with each trajectory point can be obtained by minimizing the squared difference between the reconstructed and predicted ionization charge. A parameterized model is used to predict the measured charge taking into account the diffusion of ionization electrons during transportation and the smearing of the charge distribution in subsequent signal processing. This two-step procedure is adopted to avoid a nonlinear fitting process, ensuring the stability of the fit. Regularization on smoothness is included to further improve the dQ/dx fitting performance.

The third largest background is categorized as light-mismatched events in which the measured light pattern is not consistent with the predicted light pattern from the matched TPC clusters. The consistency is examined by a Kolmogorov-Smirnov (KS) test [47]. A dedicated light-mismatch tagger [41] is used to remove various light-mismatched events with regard to: low visible energy events with short track lengths or small predicted PE signal, mismatched events caused by the inefficiency of the light detection system for cathode-side events which have

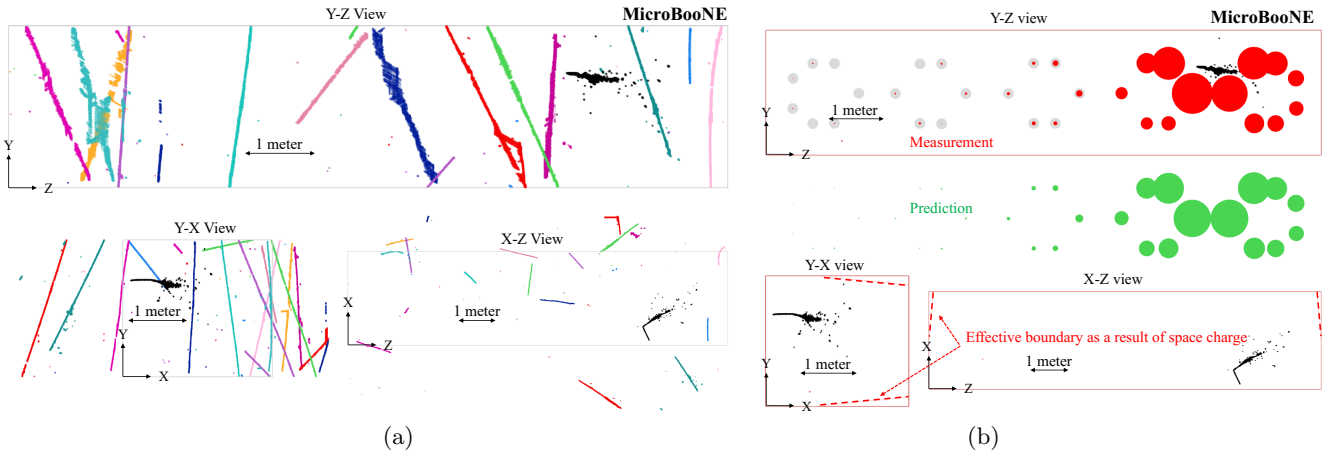

FIG. 1. A ν_e charged current (CC) interaction candidate from MicroBooNE data. The X axis is drift electric field direction from the TPC anode to the cathode. The Y axis is vertical up, and the Z axis is along the neutrino beam direction. Panel (a) shows three projections of reconstructed 3D clusters in the full TPC readout window before TPC-charge/PMT-light matching. Each cluster is shown in a different color. The gray box represents the TPC active volume while the two ends along the X axis represent the trigger time and the maximum drift time relative to the trigger. Panel (b) shows the projections of the ν_eCC candidate cluster after applying the TPC-charge/PMT-light matching. The red (green) circles represent the observed (predicted) PEs at each PMT with their area proportional to the PE. The consistency between the measured and predicted light pattern indicates a good match. The effective detector boundary as a result of space charge effects is indicated by the red dashed lines in the corner of the TPC active volume as shown in the "Y-X view" and "X-Z view".

low light acceptance for PMTs behind the anode plane, mismatched events caused by the incomplete prediction of light production originating from activities outside the TPC active volume, and incorrectly matched events that coincidentally have a reasonably good predicted and measured light pattern match. For light-mismatched events, both the light and topology information is used to seek a different TPC cluster that agrees with the measured light pattern and is consistent with a boundary-crossing muon. The external cosmic-ray tagger [48] system may provide additional rejection of the light-mismatched events but is not included in this work.

Table I summarizes the performance of the cosmic-ray background rejection and the corresponding neutrino selection efficiency for each step described previously, where the "light filter" step combines both the software trigger and the offline flash reconstruction. An overall 1.4×10^5 rejection factor is achieved, leading to a cosmic-ray impurity of 9.7% (14.9%) for reconstructed visible energy, E_{vis}, greater than 200 (0) MeV as shown in Fig. 2. E_{vis} is converted from the total charge measured from the collection plane taking into account the recombination and attenuation of the ionization electrons [41]. In addition, these algorithms retain a high fraction of the neutrino interactions originating in the fiducial volume with 88.4% (80.4%) of ν_μ charged current (CC) neutrino interactions and 80.8% (35.9%) ν_μ neutral current (NC) neutrino interactions remaining for E_{vis} greater than 200 (0) MeV. The loss of NC interactions below 200 MeV is due to the large fraction of NC interactions without easily reconstructable low energy hadronic final state.

The selected events from beam-on MC simulation and beam-off data samples are compared to the selected events from a beam-on data sample, as shown in Fig. 2. Each event has a neutrino interaction in this beam-on MC sample. All reported numbers are scaled to a BNB exposure of 5×10^{19} POT. The error bars are statistical only for both data and MC samples. The selected simulated neutrino events are categorized based on their interaction types and locations, including inside the fiducial volume (FV), inside the nonfunctional liquid argon volume (cryo), and outside the liquid argon volume (dirt). The main cosmic-ray background that coincides in time with the beam spill is estimated from the beam-off data sample. An additional cosmic-ray background corresponds to a cosmic-ray cluster incorrectly matched to the neutrino-induced PMT flash. This happens when the neutrino-induced signals reside largely outside the TPC active volume while still producing a sizable amount of scintillation light in the liquid argon. This type of cosmic-ray background is estimated from the beam-on MC sample.

In summary, the work presented in this letter using strictly TPC and PMT information marks a major milestone toward fully achieving the scientific goals of LArTPC neutrino oscillation experiments operating near the surface. The performance of the cosmic-ray background rejection and the generic neutrino selection efficiency is significantly improved compared to previous results [25–28]. In this work, the overall selection efficiency of inclusive ν_μ CC events in the fiducial volume is 80.4% (88.4%), with an overall cosmic contamination

TABLE I. Summary of the cosmic-ray background rejection power, the cumulative selection efficiency for neutrino interactions in the fiducial volume (94.2% of the active volume), and the neutrino signal to the cosmic-ray background ratio for each selection criterion. The relative cosmic-ray rejection power to the previous criterion is shown in parentheses. The numbers come from MC simulation of BNB neutrino interactions or beam-off data. The errors are statistical only. Neutrinos originating outside the fiducial volume are not counted in this table. See Fig. 2 for more details of the selected neutrino candidates.

Selection	ν_μ CC efficiency	ν_μ NC efficiency	cosmic-ray reduction	ν_μ : cosmic-ray
Hardware trigger	100%	100%	1 (1)	1 : 20000
Light filter	(98.31±0.03)%	(85.4±0.1)%	$(0.998\pm0.002)\times10^{-2}$ (0.01)	1 : 210
Charge-light matching	(92.1±0.1)%	(53.6±0.2)%	$(2.62\pm0.04)\times10^{-4}$ (0.026)	1 : 6.4
Through-going muon rejection	(88.9±0.1)%	(52.1±0.2)%	$(4.4\pm0.2)\times10^{-5}$ (0.17)	1.1 : 1
Stopped muon rejection	(82.9±0.1)%	(50.3±0.2)%	$(1.4\pm0.1)\times10^{-5}$ (0.32)	2.8 : 1
Light-mismatch rejection	(80.4±0.1)%	(35.9±0.2)%	$(6.9\pm0.6)\times10^{-6}$ (0.50)	5.2 : 1

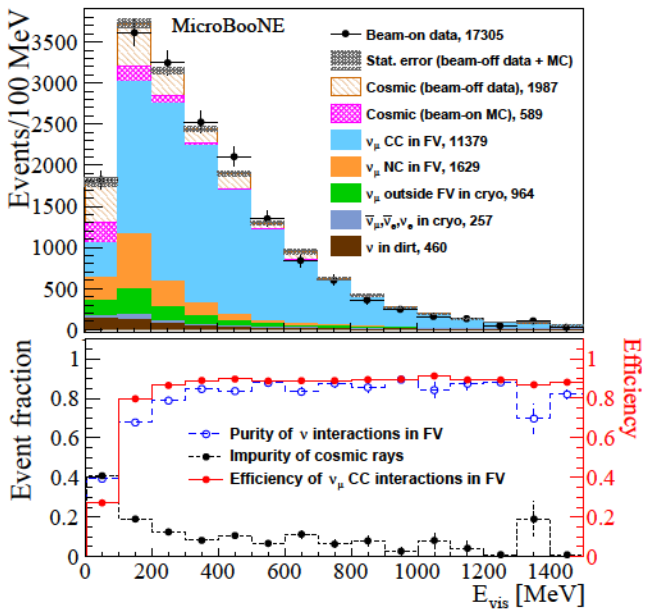

FIG. 2. Top: The selected events from the BNB beam-on data sample as a function of visible energy reconstructed in the detector are compared to the stacked selected events from beam-on MC simulation and beam-off data samples. All scaled to 5×10^{19} POT. Each event in the MC sample is guaranteed to have a neutrino interaction in the active volume or in the cryo. The selected neutrino events are categorized using the MC truth information. Bottom: The selection efficiency of ν_μ CC events originating in the fiducial volume and the event fraction for neutrino signal or cosmic-ray background are shown. The dip/jump in "purity" and "impurity" around 1400 MeV is believed to be caused by the statistical fluctuation of cosmic-ray background events in that bin.

of 14.9% (9.7%), for visible energies greater than 0 (200) MeV. About 99.98% of cosmic-ray backgrounds are rejected after software triggering. Compared to the result in Ref. [28], the overall selection efficiency of inclusive ν_μ CC events in the TPC active volume is increased by a factor of 2.7, with an enlargement of the fiducial volume by a factor of 1.9 and a reduction of the cosmic contamination by a factor of 2.4. Meanwhile, only about 10% ν_e CC events are rejected as discussed in Ref. [41]. Since many LArTPC based neutrino oscillation experiments will be statistics limited the work presented here describes a technique which significantly increases sample sizes therefore improving the sensitivity, precision and effectiveness of these detectors. The generic neutrino detection forms a solid foundation for a high-performance ν_eCC and ν_μCC event selection allowing for a compelling test of ν_e explanation of MiniBooNE low-energy excess [49] and high-precision multi-fold differential charged-current ν_μ-Ar cross section measurements. Looking forward, many of the novel techniques summarized in this work including the 3D image reconstruction, many-to-many charge-light matching, and track trajectory and dQ/dx fitting can be naturally adopted into and expected to have a significant performance impact on the upcoming SBN [19] and DUNE [20] experiments.

This document was prepared by the MicroBooNE collaboration using the resources of Fermi National Accelerator Laboratory (Fermilab), a U.S. Department of Energy, Office of Science, HEP User Facility. Fermilab is managed by Fermi Research Alliance, LLC (FRA), acting under Contract No. DE-AC02-07CH11359. MicroBooNE is supported by the following: the U.S. Department of Energy, Office of Science, Offices of High Energy Physics and Nuclear Physics; the U.S. National Science Foundation; the Swiss National Science Foundation; the Science and Technology Facilities Council (STFC), part of the United Kingdom Research and Innovation; and The Royal Society (United Kingdom). Additional support for the laser calibration system and cosmic-ray tagger was provided by the Albert Einstein Center for Fundamental Physics, Bern, Switzerland.

* microboone_info@fnal.gov

[1] C. Rubbia, "The Liquid Argon Time Projection Chamber: A New Concept for Neutrino Detectors," CERN-EP-INT-77-08, CERN-EP-77-08 (1977).

[2] H. H. Chen, P. E. Condon, B. C. Barish, and F. J. Sciulli, "A Neutrino detector sensitive to rare processes. I. A Study of neutrino electron reactions," FERMILAB-PROPOSAL-0496 (1976).

[3] W.J. Willis and V. Radeka, "Liquid Argon Ionization Chambers as Total Absorption Detectors," Nucl. Instrum. Meth. **120**, 221–236 (1974).

[4] D.R. Nygren, "The Time Projection Chamber: A New 4 pi Detector for Charged Particles," eConf **C740805**, 58 (1974).

[5] M.A. Acero *et al.* (NOvA), "First Measurement of Neutrino Oscillation Parameters using Neutrinos and Antineutrinos by NOvA," Phys. Rev. Lett. **123**, 151803 (2019), arXiv:1906.04907 [hep-ex].

[6] K. Abe *et al.* (T2K), "Constraint on the matter–antimatter symmetry-violating phase in neutrino oscillations," Nature **580**, 339–344 (2020), [Erratum: Nature 583, E16 (2020)], arXiv:1910.03887 [hep-ex].

[7] X. Qian and P. Vogel, "Neutrino Mass Hierarchy," Prog. Part. Nucl. Phys. **83**, 1–30 (2015).

[8] Pedro AN Machado, Ornella Palamara, and David W Schmitz, "The Short-Baseline Neutrino Program at Fermilab," Ann. Rev. Nucl. Part. Sci. **69** (2019).

[9] Particle Data Group, "Review of Particle Physics: Chapter 51. Neutrino Cross Section Measurements," Progress of Theoretical and Experimental Physics **2020** (2020), 10.1093/ptep/ptaa104.

[10] F. Cavanna, A. Ereditato, and B. T. Fleming, "Advances in liquid argon detectors," Nucl. Instrum. Meth. **A907**, 1–8 (2018).

[11] S. Amerio *et al.* (ICARUS Collaboration), "Design, construction and tests of the ICARUS T600 detector," Nucl. Instrum. Meth. A **527**, 329–410 (2004).

[12] C. Anderson *et al.* (ArgoNeuT Collaboration), "The ArgoNeuT Detector in the NuMI Low-Energy beam line at Fermilab," JINST **7**, P10019 (2012).

[13] R. Acciarri *et al.* (MicroBooNE Collaboration), "Design and Construction of the MicroBooNE Detector," JINST **12**, P02017 (2017).

[14] I. Badhrees *et al.*, "Argontube: An R&D liquid Argon Time Projection Chamber," JINST **7**, C02011 (2012).

[15] B. Bhandari *et al.* (CAPTAIN Collaboration), "First Measurement of the Total Neutron Cross Section on Argon Between 100 and 800 MeV," Phys. Rev. Lett. **123**, 042502 (2019).

[16] Alan Hahn *et al.* (LBNE Collaboration), "The LBNE 35 Ton Prototype Cryostat," in *2014 IEEE Nuclear Science Symposium and Medical Imaging Conference and 21st Symposium on Room-Temperature Semiconductor X-ray and Gamma-ray Detectors* (2016) p. 7431158.

[17] J. Paley *et al.* (LArIAT Collaboration), "LArIAT: Liquid Argon In A Testbeam," (2014), arXiv:1406.5560 [physics.ins-det].

[18] B. Abi *et al.* (DUNE Collaboration), "First results on ProtoDUNE-SP liquid argon time projection chamber performance from a beam test at the CERN Neutrino Platform," JINST **15**, P12004 (2020), arXiv:2007.06722 [physics.ins-det].

[19] M. Antonello *et al.* (MicroBooNE, LAr1-ND, and ICARUS-WA104 Collaboration), "A Proposal for a Three Detector Short-Baseline Neutrino Oscillation Program in the Fermilab Booster Neutrino Beam," (2015), arXiv:1503.01520 [physics.ins-det].

[20] Babak Abi *et al.* (DUNE Collaboration), "Deep Underground Neutrino Experiment (DUNE), Far Detector Technical Design Report, Volume I Introduction to DUNE," JINST **15**, T08008 (2020).

[21] A. A. Aguilar-Arevalo *et al.* (MiniBooNE Collaboration), "The Neutrino Flux prediction at MiniBooNE," Phys. Rev. D. **79**, 072002 (2009).

[22] T. Briese *et al.*, "Testing of Cryogenic Photomultiplier Tubes for the MicroBooNE Experiment," JINST **8**, T07005 (2013), arXiv:1304.0821 [physics.ins-det].

[23] Veljko Radeka *et al.*, "Cold electronics for 'Giant' Liquid Argon Time Projection Chambers," *Giant liquid argon charge imaging experiment. Proceedings, 1st International Workshop, GLA2010, Tsukuba, Japan, March 29-31, 2010*, J. Phys. Conf. Ser. **308**, 012021 (2011).

[24] R. Acciarri *et al.* (MicroBooNE Collaboration), "Measurement of cosmic-ray reconstruction efficiencies in the MicroBooNE LArTPC using a small external cosmic-ray counter," JINST **12**, P12030 (2017).

[25] C. Adams *et al.* (MicroBooNE Collaboration), "Comparison of ν_μ-Ar multiplicity distributions observed by MicroBooNE to GENIE model predictions," Eur. Phys. J. **C79**, 248 (2019).

[26] C. Adams *et al.* (MicroBooNE Collaboration), "First measurement of ν_μ charged-current π^0 production on argon with the MicroBooNE detector," Phys. Rev. **D99**, 091102 (2019).

[27] C. Adams *et al.* (MicroBooNE Collaboration), "Rejecting cosmic background for exclusive charged current quasi elastic neutrino interaction studies with Liquid Argon TPCs; a case study with the MicroBooNE detector," Eur. Phys. J. **C79**, 673 (2019).

[28] P. Abratenko *et al.* (MicroBooNE Collaboration), "First Measurement of Inclusive Muon Neutrino Charged Current Differential Cross Sections on Argon at $E_\nu \sim$0.8 GeV with the MicroBooNE Detector," Phys. Rev. Lett. **123**, 131801 (2019).

[29] R. Acciarri *et al.* (MicroBooNE Collaboration), "Noise Characterization and Filtering in the MicroBooNE Liquid Argon TPC," JINST **12**, P08003 (2017).

[30] C. Adams *et al.* (MicroBooNE Collaboration), "Ionization electron signal processing in single phase LArTPCs. Part I. Algorithm Description and quantitative evaluation with MicroBooNE simulation," JINST **13**, P07006–P07006 (2018).

[31] Bruce Baller, "Liquid argon TPC signal formation, signal processing and reconstruction techniques," JINST **12**, P07010 (2017).

[32] C. Adams *et al.* (MicroBooNE Collaboration), "Ionization electron signal processing in single phase LArTPCs. Part II. Data/simulation comparison and performance in MicroBooNE," JINST **13**, P07007 (2018).

[33] Xin Qian, Chao Zhang, Brett Viren, and Milind Diwan, "Three-dimensional Imaging for Large LArTPCs," JINST **13**, P05032 (2018).

[34] P. Abratenko *et al.* (MicroBooNE), "Neutrino Event Selection in the MicroBooNE Liquid Argon Time Projection Chamber using Wire-Cell 3-D Imaging, Clustering, and Charge-Light Matching," (2020), accepted by JINST, arXiv:2011.01375 [physics.ins-det].

[35] P. Adamson *et al.* (NOvA Collaboration), "First measurement of muon-neutrino disappearance in NOvA," Phys. Rev. **D93**, 051104 (2016).

[36] L. Aliaga *et al.* (MINERvA Collaboration), "Design, Calibration, and Performance of the MINERvA Detector,"

Nucl. Instrum. Meth. **A743**, 130–159 (2014).

[37] D. G. Michael *et al.* (MINOS Collaboration), "The Magnetized steel and scintillator calorimeters of the MINOS experiment," Nucl. Instrum. Meth. **A596**, 190–228 (2008).

[38] S. Agostinelli *et al.*, "GEAnt4–a simulation toolkit," Nucl. Instrum. Methods Phys. Res. **Sect. A 506**, 250 (2003).

[39] J. Allison *et al.*, "Geant4 developments and applications," IEEE Trans. Nucl. Sci. **53**, 270 (2006).

[40] E. J. Candès, J. K. Romberg, and T. Tao, "Stable signal recovery from incomplete and inaccurate measurements," Communications on Pure and Applied Mathematics **59**, 1207–1223 (2006).

[41] P. Abratenko *et al.* (MicroBooNE Collaboration), "Cosmic Ray Background Rejection with Wire-Cell LArTPC Event Reconstruction in the MicroBooNE Detector," (2020), submitted to Physical Review Applied.

[42] C. Adams *et al.* (MicroBooNE Collaboration), "A Method to Determine the Electric Field of Liquid Argon Time Projection Chambers Using a UV Laser System and its Application in MicroBooNE," JINST **15**, P07010 (2020).

[43] P. Abratenko *et al.* (MicroBooNE), "Measurement of space charge effects in the MicroBooNE LArTPC using cosmic muons," JINST **15**, P12037 (2020), arXiv:2008.09765 [physics.ins-det].

[44] M. Antonello *et al.*, "Precise 3D track reconstruction algorithm for the ICARUS T600 liquid argon time projection chamber detector," Adv. High Energy Phys. **2013**, 260820 (2013).

[45] "Steiner tree greedy algorithm," `http://paal.mimuw.edu.pl/docs/index.html` (2019).

[46] "Biconjugate gradient stablized method (BiCGSTAB)," `https://eigen.tuxfamily.org/dox/classEigen_1_1BiCGSTAB.html` (2019).

[47] A. Kolmogorov, "Sulla determinazione empirica di una legge di distribuzione," G. Ist. Ital. Attuari **4**, 83 (1933).

[48] C. Adams *et al.* (MicroBooNE Collaboration), "Design and construction of the MicroBooNE Cosmic Ray Tagger system," JINST **14**, P04004 (2019).

[49] A. A. Aguilar-Arevalo *et al.* (MiniBooNE), "Updated MiniBooNE Neutrino Oscillation Results with Increased Data and New Background Studies," (2020), arXiv:2006.16883 [hep-ex].